Effect of phase change on shock wave attenuation in GeO_2

C. Liu[a] and T. J. Ahrens
Seismological Laboratory 252-21, California Institute of Technology, Pasadena, California 91125

N. S. Brar
University of Dayton Research Institute, Dayton, Ohio 45469-0182

(Received 22 October 2001; accepted for publication 22 February 2002)

Stress-wave profiles in vitreous GeO_2 induced by planar and spherical projectile impact were measured using piezoresistance gauges in the 4 to 18 GPa shock pressure range. The planar experiments demonstrate the response of vitreous GeO_2. This response can be divided into three regimes: (1) An elastic shock regime with ramp 4 GPa Hugoniot elastic limit (HEL) precursor. Shock propagation velocity decreases from an initial longitudinal elastic wave speed of 3.5 to 2.8 km/s at 4 GPa. (2) A transition wave regime where the ramp wave is superimposed on the precursor with an additional amplitude of 0 to 2 GPa followed by a sharp increase in shock pressure achieving peak loading pressures of 8 to 14 GPa. Above 4 GPa the ramp wave velocity decreases to a value below 2.5 km/s (the speed of the bulk wave, at the HEL). (3) A shock wave achieving the final shock state forms when peak pressure is >6 GPa specified by linear shock-particle velocity relation $D=0.917+1.71\ u$ (km/s) over the 6–40 GPa range for an initial density of 3.655 g/cm^3. The Hugoniots of GeO_2 and SiO_2, both initially vitreous, are found to be virtually coincident if pressure in SiO_2 is calculated by multiplying the GeO_2 pressure by the ratio of the initial densities of vitreous GeO_2 to fused SiO_2. The volume axes are translated by aligning the specific volumes for onset and completion of the four- to six-fold coordination phase change. Although only limited spherical impactor spherically diverging shock experiments were conducted, our present results demonstrate (1) The supported elastic shock in fused SiO_2 decays less rapidly than a linear elastic wave when elastic wave stress amplitude is higher than 4 GPa. A supported elastic precursor in vitreous GeO_2 decays faster with radius than a linear elastic wave; (2) in GeO_2 (vitreous) unsupported shock waves decay with peak pressure in a phase transition range (4–15 GPa) with propagation radius (r) as $\propto r^{-3.35}$. © *2002 American Institute of Physics.* [DOI: 10.1063/1.1469663]

I. INTRODUCTION

In the 1960s and early 1970s when the first shock wave measurements were conducted on silicates,[1–5] it became clear that this class of materials all demonstrated behavior that indicated transformation to dense structures in which Si^{+4} was coordinated to six O^{-2} ions. This is the coordination observed in the high-pressure phase of SiO_2, stishovite (rutile-structured phase) which has a density of 4.30g/cm^3, some 62% and 95% greater than crystal or fused quartz starting materials.[6] Motivated by scientific curiosity, a need to contain underground testing products and understand the interaction with rock of nuclear explosions in the Earth, a detailed series of shock measurements on SiO_2 and other silicate minerals were conducted.[7–9] These studies pointed to the general conclusion that transformation to the high-pressure phase occurred upon overdriving the low-pressure phase to a significantly higher shock pressure than required for thermodynamic equilibrium by, in several cases, a factor of 2. Although a multiwave structure for the transformation of Si^{+4} from four- to sixfold coordination has long been anticipated, in the case of dynamic compression of crystal quartz, this has only recently been observed by Ref. 10.

Unloading, from the mixed phase and/or high-pressure phase regimes demonstrated highly hysteretic behavior. Unloading takes place along a pressure-density path characteristic of the high-pressure phase and, as a result of this hysteresis, the silicates appeared to be extremely absorptive of shock energy, upon propagation at stress levels above those required for polymorphic transformation, e.g., Swegle.[11] Moreover, only recently have we understood this behavior in terms of the inclusion theory of Truskinovsky.[12] Turnbull[13] developed a theory to describe quasistatic transformation which is expected to be applicable to many shock-induced transformations, including the quartz-stishovite transformation[14] because it is martinsitic in nature as are other major and important phase changes such as the $\alpha \rightarrow \epsilon$ phase (iron), $B1 \rightarrow B2$ phase (alkali halides), and graphite $\rightarrow$diamond.

Although it was long recognized that the phase transformation in silicates and SiO_2 occurred at stress levels of $\sim$10–20 GPa, this stress level and hence these transformations were out of range of interest of light armor materials.

However, in the case of GeO_2 and other germenates this does not seem to be the case. For GeO_2 (which has a phase diagram similar to SiO_2) the glass (3.64 g/cm^3) to rutilelike phase (6.25 g/cm^3) transformation demonstrates a density increase of 72% that occurs over the pressure range of 4–13 GPa as inferred by previous studies using various experi-

[a]Present address: Southwest Institute of Fluid Physics, Sichuan 621900, People's Republic of China.

 © 2002 American Institute of Physics

Downloaded 21 Dec 2005 to 131.215.225.171. Redistribution subject to AIP license or copyright, see http://jap.aip.org/jap/copyright.jsp

mental methods.[15–17] This shock stress range previously delineated by Jackson and Ahrens[18] is confirmed by the present work. Previously[18] Hugoniot data up to 160 GPa were obtained. These data suggested that both vitreous and rutile phases transform to a common phase under high pressure, which is about 5% denser than the rutile-type structure. Release isentropic measurements by Chen *et al.*[19] implied that vitreous GeO_2 undergoes an irreversible phase change above 8 GPa. Research on GeO_2 phase transitions and their effect on shock wave decay helps to understand the silicate phase transition effect on the shock wave decay rate that has not been fully studied.[20] Based on an irreversible phase transition model constructed from data on shock compression of vitreous GeO_2, Chen *et al.*[19] predicted that unsupported shock waves, with pressures greater than 8 GPa, decay significantly more rapidly than unsupported shock waves with pressure below 8 GPa.

In the present article, we describe new measurements of shock structure and attenuation in GeO_2 and SiO_2 in one-dimensional longitudinal compression and upon propagation in a spherical diverging, unsupported shock geometry.

II. EXPERIMENTAL METHOD

We chose to measure stress wave profiles in the present experiments as these define material deformation processes. The processes of interest include dynamic yielding, elastic–plastic deformation, phase transformation, and the resulting enhanced shock wave attenuation. Embedded piezoresistance manganin stress gauges (e.g., Ref. 21) were employed to monitor stress wave profiles under planar and spherical projectile impact.

A. Sample preparation

A cylinder (100 mm diameter and 150 mm in height) of bubble-free vitreous GeO_2 (Corning, Inc.) was cut into 40 $\times$40 mm square samples with thicknesses of 1.7 to 10 mm. The bulk density is measured to be 3.655 g/cm^3. Samples were first polished to within 0.005 mm of uniform thickness. Then, stress gauges mounted on mylar film (0.013 mm thickness) were sandwiched between two samples. Epoxy was used to force air out of the contact surfaces between the gauges or samples and mylar film. After the epoxy cured (typically 24 h), the whole sample assembly was encapsulated in epoxy as shown in Fig. 1.

B. Planar impact

In order to generate uniaxial strain shock waves, planar impactors (Fig. 1) were launched against GeO_2 samples. Under the assumption that the relation between stress change and gauge resistance change is not sample material dependent, the relation between normal stress $\sigma(t)$, and manganin stress gauge resistance change $dR(t)$ was assumed as follows:[21]

$$\sigma(t)=A_0+A_1 dR(t)+A_2 dR^2(t)+A_3 dR^3(t)+A_4 dR^4(t), \quad (2.1)$$

where $dR(t)=[R(t)-R_0]/R_0$. Here $R(t)$ is gauge resistance at time t and R_0 is initial gauge resistance, 50 Ω. The parameters, A_i are assumed to be constant. When $\sigma \leqslant 1.5$ GPa, $A_1=50$ (GPa) and all the others are zero. When $\sigma \geqslant 1.5$ GPa, $A_0=0.572$ GPa, $A_1=29.59$ GPa, $A_2=95.20$ GPa, $A_3=-312.74$ GPa, and $A_4=331.77$ GPa. The four manganin stress gauges (Mn-4-50-ER, Dynasen, Inc.) used in each experiment were powered by two-channel power supplies (CK-2, Dynasen, Inc.) with built-in preamplifers. These were mounted among three GeO_2 samples in each experiment. Digital oscilloscopes (HP54502, HP) were used to record the voltage output from the preamplifiers. Voltage is converted to gauge resistance using the calibrated relations between resistance change and voltage output (Ref. 22). Stress wave profiles are then calculated using Eq. (2.1).

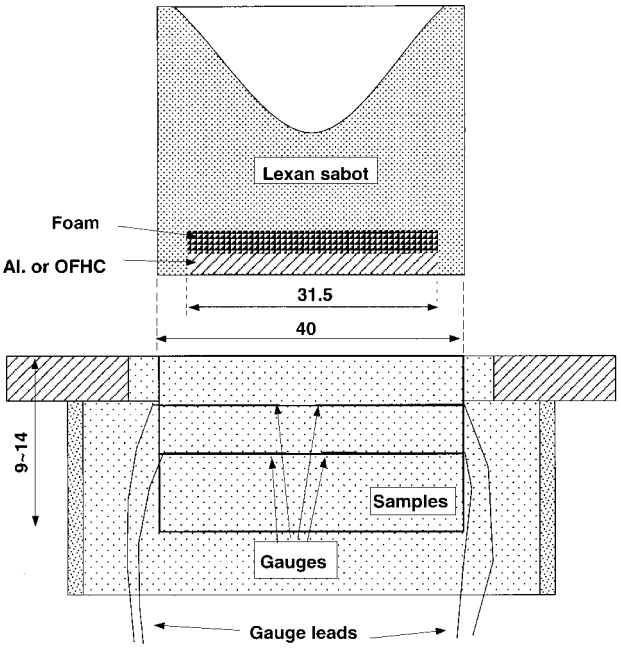

FIG. 1. Target assembly. All dimensions are in mm.

C. Spherical projectile impact

In order to investigate phase transition effects upon unsupported shock wave propagation, spherical projectile (Fig. 2) impact experiments were conducted on vitreous GeO_2 and fused SiO_2. The stress profiles under spherical projectile im-

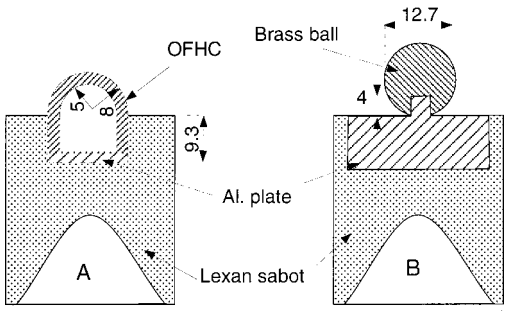

FIG. 2. Spherical projectile (A) for shot 1030 and 1031 and (B) for shot 1023. All dimensions are in mm.

Downloaded 21 Dec 2005 to 131.215.225.171. Redistribution subject to AIP license or copyright, see http://jap.aip.org/jap/copyright.jsp

pact were measured using a combination of piezoresistance Mn-4-50-ER stress gauges and strain gauges (Cn-4-50-ER, Dynasen Inc.). This stress and strain gauge combination employed manganin to measure stress and constantan to measure strain in approximately the same geometry. Under nonplanar shock wave loading, manganin stress gauge resistance change dR_{Mn} has two components: one is the resistance change due to stress, $dR_{\mathrm{Mn\text{-}stress}}$, and the second is the resistance change due to strain along gauge direction, $dR_{\mathrm{Mn\text{-}strain}}$ (Fig. 3). However, constantan strain gauge resistance change dR_{Cn} results only from strain along gauge direction because constantan gauge resistance does not (to a first approximation) depend on stress. Therefore, strain ϵ along gauge direction measured by strain gauges is

$$\varepsilon = \frac{dR_{\mathrm{Cn}}}{G_{\mathrm{Cn}} R_{\mathrm{CnO}}}, \tag{2.2}$$

where G_{Cn} is the strain factor and R_{Cn0} is initial strain gauge resistance, 50 Ω. We assume that the stress gauge resistance change is a linear combination of stress and strain induced resistance changes

$$dR_{\mathrm{Mn}} = dR_{\mathrm{Mn-stress}} + dR_{\mathrm{Mn\text{-}strain}}. \tag{2.3}$$

Then, stress gauge resistance change related to stress is

$$dR_{\mathrm{Mn\text{-}stress}} = dR_{\mathrm{Mn}} - dR_{\mathrm{Mn\text{-}strain}}. \tag{2.4}$$

Because $dR_{\mathrm{Mn\text{-}strain}} = G_{\mathrm{Mn}} \varepsilon R_0$, Eq. (2.4) becomes

$$dR_{\mathrm{Mn\text{-}stress}} = dR_{\mathrm{Mn}} - G_{\mathrm{Mn}} \varepsilon R_0, \tag{2.5}$$

where G_{Mn} is the strain factor of manganin stress gauge. G_{Mn} and G_{Cn} are calibrated experimentally and vary from 1.0 to 2.1 as strain varies from 0% to 5%. In each experiment, two piezoresistance stress and two strain gauges were used to monitor stress wave profiles at two interfaces among three samples.

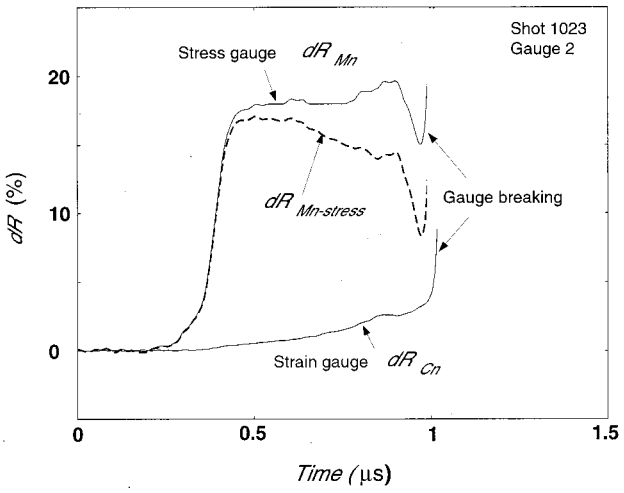

FIG. 3. Typical stress-strain gauge resistance change profiles, shot 1023.

III. EXPERIMENTAL RESULTS

A. Planar impact results

The recorded stress-wave profiles in vitreous GeO_2 (Table I, Fig. 4) show that the two stress gauges at the same interface yield nearly identical stress wave fronts, and displayed only minor differences in the peak stress behind the wave front.[21] Wave profiles shown in Fig. 4 appear to display a three-wave structure: an elastic precursor with relative long rise time, a ramp wave, and then a normal shock wave when the peak stress is >6 GPa. Because each wave is related to a different dynamic process, the parameters of each wave are determined using relations with slightly different approximations as discussed below.

1. Elastic precursor parameters

The precursor rise time is ~100 and 150 ns at 1.8 and 4.2 mm from impact surface (Fig. 5), respectively. In order to verify that this rise time is not the response of the measurement system, Fig. 5 provides a comparison among the wave profiles that are aligned with respect to arrival time and dem-

TABLE I. Experimental parameters for planar and spherical impact experiments.

Shot No.	Impactor material	Impactor thickness (mm)	Impactor velocity (km/s)	H_1 (mm)	H_2 (mm)	H_3 (mm)
Planar experiments						
1024	OFHC	5.997±0.001	1.547±0.006	1.857±0.0041	1.745±0.0034	10.378
1026	2024 Al.	4.02±0.001	2.062±0.013	2.454±0.0021	2.238±0.0019	5.883
1027	2024 Al.	6.015±0.005	2.310±0.001	2.202±0.0038	2.588±0.0021	6.192
1028	2024 Al.	6.021±0.0043	1.304±0.001	1.836±0.004	2.360±0.005	5.298
Spherical experiments						
Shot No.	Impactor material	Impactor diameter (mm)	Impactor velocity (km/s)	H_1 (mm)	H_2 (mm)	H_3 (mm)
1023	OFHC	16	1.302±0.01	6.294±0.009	6.462±0.003	4.86
1030	Brass	12.722±0.0018	1.709±0.006	5.408±0.003	5.377±0.006	5.873
1031	Brass	12.715±0.001	1.695±0.011	3.312±0.004	4.877±0.003	5.832

H_1, H_2, and H_3 are thicknesses of three samples in each experiment. Shot 1023 target material is fused SiO_2 with initial density 2.203 g/cm^3. The 2024 aluminum plate was in front of target materials of shot 1023. A 9 mm hemispherical cavity, with a depth of 2.5 mm, was on the impact surface of plate.

Downloaded 21 Dec 2005 to 131.215.225.171. Redistribution subject to AIP license or copyright, see http://jap.aip.org/jap/copyright.jsp

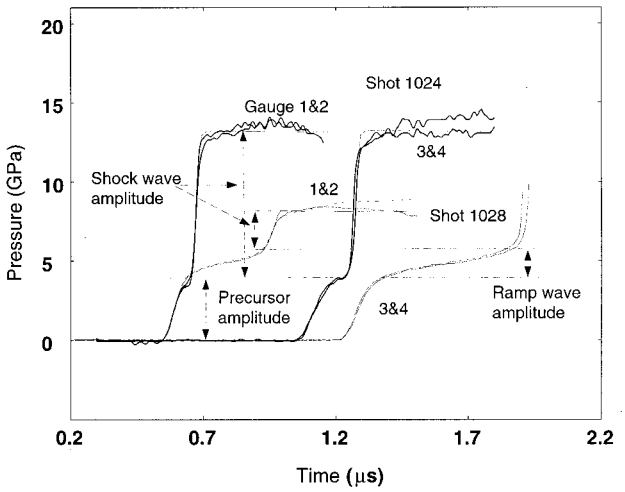

FIG. 4. Typical stress-wave profiles in vitreous GeO_2, shot 1024.

onstrates that the precursor rise time increases with propagation distance. As a result, we infer that the longitudinal modulus of vitreous GeO_2 decreases with increasing stress during precursor wave loading and the precursor is an elastic ramp (spreading) wave. Because the deformation rate associated with ramp wave loading is less than for shock wave loading, we approximate this process by assuming isentropic compression. Since the precursor stress does not appear to decay with propagation distance (Fig. 5), we assume, the phase velocity at constant particle velocity and stress are equal.[2] We use the Fowles and Williams[2] procedure to calculate the precursor parameters. We divide the ramp wave into a series of small stress increments $\delta\sigma$ and treat each stress increment as a wave with stress jump $\delta\sigma$, particle velocity change δu, and specific volume change δV. These parameters for each increment are then related by

$$\delta u = \frac{\delta\sigma}{\rho_0 C_\sigma}, \quad \delta V = -\frac{\delta u}{\rho_0 C_\sigma}, \tag{3.1}$$

where ρ_0 is initial density, and C_σ is wave velocity at stress σ. C_σ is given by $(\partial H/\partial t)_\sigma \approx H_2/(t_2 - t_1)$ in which H_2 is the initial thickness of the sample between the two stress gauges, and t_2 and t_1 are wave arrival times at the two gauges, respectively. Then the Eulerian wave velocity C_e is

$$C_e = \rho_0 V C_\sigma, \tag{3.2}$$

where V is specific volume at stress σ.

Using Eqs. (3.1) and (3.2), particle velocity, specific volume, and wave velocity along the precursor loading paths and final shock states are shown in Figs. 6 and 7. The peak stress maximum propagation velocity and maximum particle velocity associated with GeO_2 precursors are summarized in Table II.

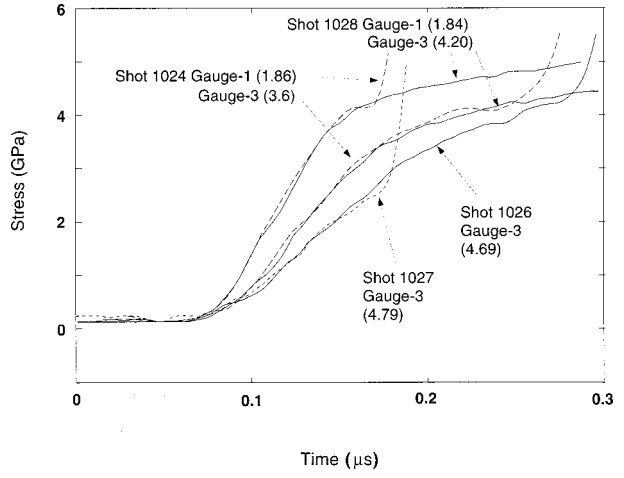

FIG. 5. Elastic wave front rise time vs propagation distance. The number in parentheses is distance (mm) between gauge and impact surface.

2. Ramp deformational wave parameters

From the recorded wave profiles of shot 1028, we conclude that uniaxial strain compressibility increases in the stress range of 4 to 6 GPa. This results in a dispersive wave. Assuming that the compression in this stress range is isentropic, Eqs. (3.1) and (3.2) are used to calculate the parameters related to the ramp wave. The stress increase associated with the ramp wave is 2.1 GPa. The wave velocity drops to 2.3 from 2.9 km/s and the particle velocity increases from 0.33 to 0.57 km/s (Fig. 6). The calculated specific volume decreases from 0.247 to 0.228 cm^3/g (Fig. 7).

3. Shock wave parameters

The parameters related to the shock wave that follows the ramp wave are deduced using the usual jump conditions:

$$D - u_b = \frac{H_b}{\Delta t},$$

$$u_1 - u_b = \frac{\sigma_1 - \sigma_b}{\rho_b (D - u_b)}, \tag{3.3}$$

$$\frac{\rho_1}{\rho_b} = \frac{D - u_b}{D - u_1},$$

where D and u are shock wave and particle velocity, respectively. ρ is density and σ is stress. H is the distance between two gauges. Δt is the time between two arrivals of the shock wave front at two gauges. The subscripts b and 1 refer to the states before and behind the shock wave front, respectively.

Because release waves from near surface of the impactor had not overtaken the shock front waves in all the present experiments, the peak stress in each experiment is assumed to be constant at two stress gauge locations. Therefore, the peak stress in each experiment is determined by averaging the peak stress from all the gauges. The peak stress data points are listed in Table III and shown in Figs. 6 and 7. A least square fit was obtained based on present and earlier[18] data. This fit describes the Hugoniot of vitreous GeO_2 in the pressure range of 6 to 40 GPa as

$$D = 0.974 + 1.711u \quad \text{for } u > 0.6 \text{ km/s}, \tag{3.4}$$

where D and u are both in km/s.

Downloaded 21 Dec 2005 to 131.215.225.171. Redistribution subject to AIP license or copyright, see http://jap.aip.org/jap/copyright.jsp

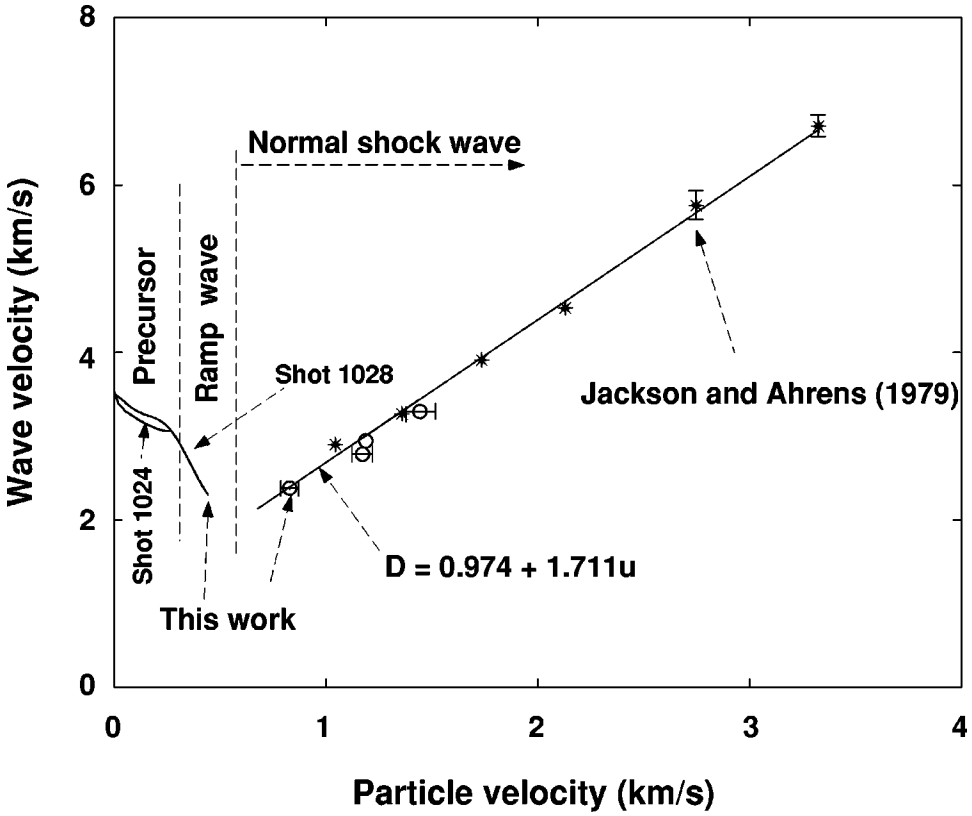

FIG. 6. Shock wave velocity vs particle velocity for GeO_2 glass, initial density 3.655 g/cm^3.

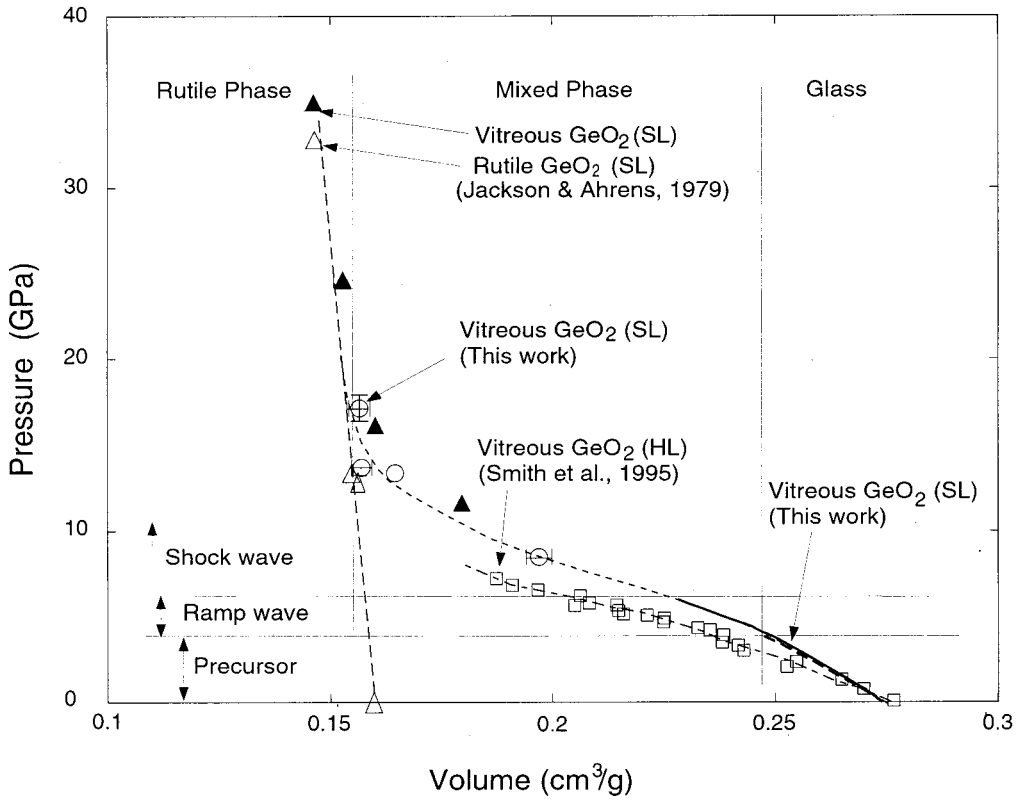

FIG. 7. Shock pressure vs volume of vitreous GeO_2. SL and HL are shock loading and hydrostatic loading, respectively. The light dashed line is schematic.

Downloaded 21 Dec 2005 to 131.215.225.171. Redistribution subject to AIP license or copyright, see http://jap.aip.org/jap/copyright.jsp

TABLE II. Experimental data of elastic precursor in GeO_2.

Shot No.	σ_e[a] (GPa)	C_{el}[b] (km/s)	u_e[c] (km/s)	ρ_e[d] g/cm^3
1024	3.82±0.17	3.50±0.09	0.315±0.015	4.04±0.024
1026	3.95±0.05	3.51±0.02		
1028	4.09±0.11	3.51±0.01	0.333±0.009	4.05±0.01

[a]σ_e, precursor peak stress.
[b]C_{el}, precursor maximum (leading edge) propagation velocity.
[c]u_e, precursor peak particle velocity.
[d]ρ_e, density at σ_e.

B. Spherical impact results for SiO_2 and GeO_2

Under spherical impact, recorded stress-wave profiles in fused SiO_2 (shot 1023) and vitreous GeO_2 (shot 1030 and 1031) are shown in Figs. 8 and 9. Experimental parameters are listed in Table I. The decays of precursor and peak shock wave amplitude with propagation distance are discussed separately in the following.

1. Precursor decay

Based on the Hugoniot relations of fused SiO_2 and Cu,[23] the peak stress at impact surface is calculated to be 11.4 GPa for the experiment on fused SiO_2. Because the Hugoniot elastic limit (HEL) of fused SiO_2 is 9.83±0.24 GPa,[1] the wave measured in shot 1023 is probably an elastic wave. The wave also appears to be supported (at gauge No. 1 and marginally at gauge No. 2), because a stress plateau behind the wave front appeared at both locations (Fig. 8). Figure 10 gives the elastic wave peak stress at each location from the experiment (elastic shock wave peak stress at the impact surface is assumed to be at the HEL). The data from two gauges taken with Wackerle's value for the fused quartz HEL, yields

$$\sigma_x^S = 9.95\left(\frac{x}{X}\right)^{-0.54}, \tag{3.5}$$

where σ_x^S, in GPa, is elastic wave peak stress at a distance x in mm from the center of a spherical projectile, and X is a spherical projectile radius. Equation (3.5) implies that the supported elastic wave in fused SiO_2 decays less rapidly than $(x/X)^{-1}$ which is the assumed elastic behavior for a spherical wave from a point source.

In the case of vitreous GeO_2, the peak pressure at the impact surface is calculated to be 14.6 and 14.4 GPa for shots 1030 and 1031, respectively, based on Eq. (3.4) and the Hugoniot of brass.[23] The stress-wave profiles in vitreous GeO_2 show a kink at just below precursor limit (indicated by arrows, 1 to 4 in Fig. 9). This kink is believed to be a remnant of the precursor formed at the impact surface. This feature forms only when wave velocity decreases with increasing stress. From the present data on vitreous GeO_2 under planar impact, the wave velocity appears to decrease with increasing stress when peak stress is below 6 GPa. Therefore, the stress amplitude at the kinks gives the decay of a supported precursor in vitreous GeO_2 (Fig. 10). A fit to the data yields

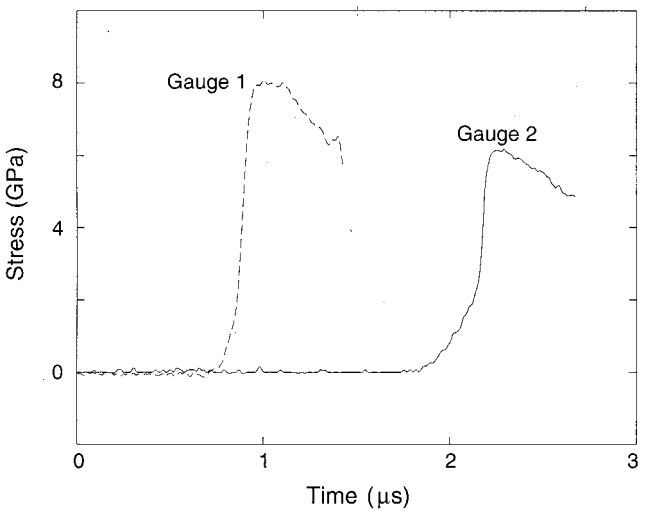

FIG. 8. Stress-wave profiles in fused SiO_2 under spherical impact.

$$\sigma_x^G = 4.06\left(\frac{x}{X}\right)^{-1.24}, \tag{3.6}$$

where σ_x^G, in GPa, is stress amplitude at the kinks. Equation (3.6) suggests that a supported elastic precursor in vitreous GeO_2 decays slightly faster than $(x/X)^{-1}$ expected for a linear elastic wave.

2. Deformational shock wave decay

The peak stress at each gauge location is indicated by a horizontal dashed line in Fig. 9. The peak stress at the first gauge of shot 1031 was determined as the gauge recorded the stress clearly. The peak stress for the first gauge in shot 1030 is less certain because the gauge appeared to fail when the stress reached its maximum value. In order to infer if the second gauge for both shots recorded the maximum stress, we estimate the time t_n after which no shock wave could arrive at the second gauge. If the possible slowest shock

TABLE III. Experimental data, shock parameters in GeO_2.

Shot No.	σ_1 (GPa)	$\sigma_1-\sigma_b$ (GPa)	D (km/s)	u_1 (km/s)	ρ_1 (g/cm^3)
1024	13.35±0.28	9.24±0.28	2.928±0.008	1.18±0.029	6.089±0.05
1026	13.65±0.39	9.24±0.39	2.777±0.029	1.164±0.048	6.386±0.097
1027	17.11±0.76	14.49±0.76	3.286±0.02	1.438±0.072	6.401±0.099
1028	8.42±0.25	2.27±0.25	2.625±0.02	0.821±0.027	5.088±0.076

Uncertainties in σ_1, $\sigma_1-\sigma_b$, and D from experiments. Uncertainties in u_1 and ρ_1 are calculated using a formula derived by differentiating Eq. (3.3).

Downloaded 21 Dec 2005 to 131.215.225.171. Redistribution subject to AIP license or copyright, see http://jap.aip.org/jap/copyright.jsp

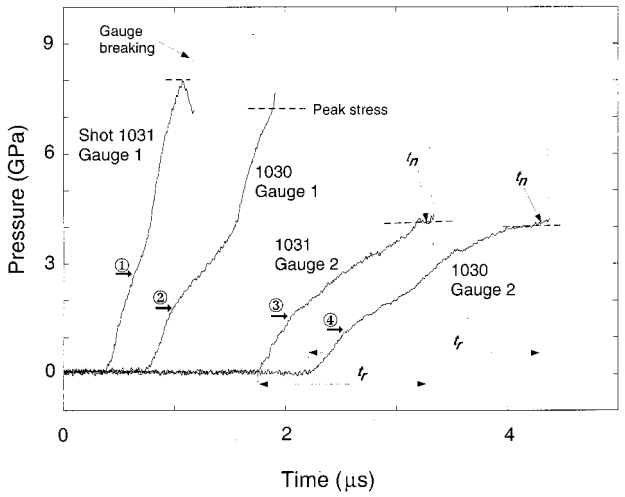

FIG. 9. Stress-wave profiles in vitreous GeO_2 under spherical impact. Four arrows indicate the remnant of elastic shock precursor originating from impact surface. t_r is wave rise time used to estimate that the distance gauge has moved before final shock arrival. t_n is the time when the final shock state is achieved. The horizontal dashed line is peak stress. The vertical dashed line indicates the breaking time of the gauge.

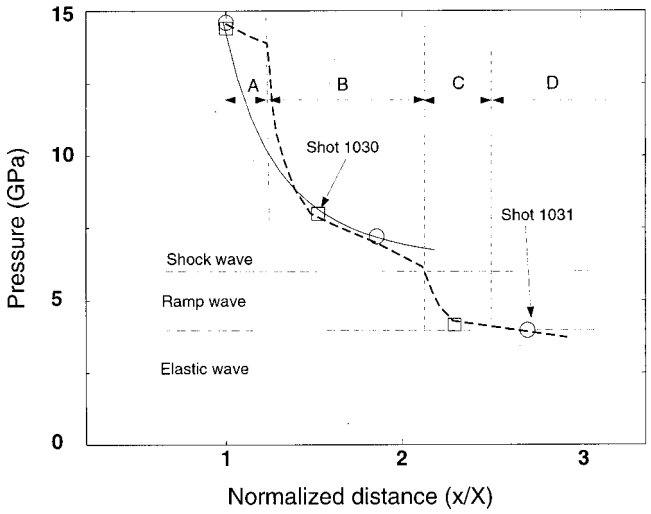

FIG. 11. Peak shock pressure vs propagation distance in GeO_2 under spherical impact. (A) Near field decay. (B) Phase transition dominated decay. (C) Ramp-wave dominated decay. (D) Elastic wave decay. The solid line is a fit to data [Eq. (3.7)]. The heavy dashed line is schematic.

wave velocity D_s is known, t_n is estimated to be H_s/D_s in which H_s is the propagation distance of the shock wave. D_s is estimated using Eq. (3.4) when $u=0.6$ km/s. H_s is approximated to be $(H_1+H_2+u_e t_r/2)$, where t_r is defined in Fig. 9. Here u_e is the maximum particle velocity of the precursor ($u_e t_r/2$ is due to gauge motion before shock wave arrives at the gauge location). The estimated time t_n is shown in Fig. 9 and demonstrates that the second gauges were recording upon arrivals of the maximum shock stress.

When peak shock stress is much higher than elastic wave amplitude, peak shock stress decay is described using the form of $(x/X)^{\alpha}$ in which x is the distance from the spherical projectile center and X is the spherical projectile radius.[20] However, when peak shock stress is comparable with elastic wave amplitude, a shock attenuation equation of the form $A+B(x/X)^{\alpha}$ is more appropriate as the peak precursor stress does not decrease rapidly with propagation distance. We assume the constant A is precursor amplitude and the second term describes the decay of the deformational shock wave with propagation distance.

The form of $A+B(x/X)^{\alpha}$ is used because the peak stress in the two experiments depicted in Fig. 11 is comparable with precursor amplitude. In order to estimate the shock wave decay in the phase transition stress range, α is assumed to be a constant. A fit to the data of shock wave stress (the difference between the peak stress and the stress just behind the ramp wave) is

$$P=6.1+8.34\left(\frac{x}{X}\right)^{-3.35}, \tag{3.7}$$

where P in GPa is peak shock stress (the sum of the precursor, ramp wave and deformational shock wave amplitudes). The second term in the above expression describes shock wave decay in vitreous GeO_2.

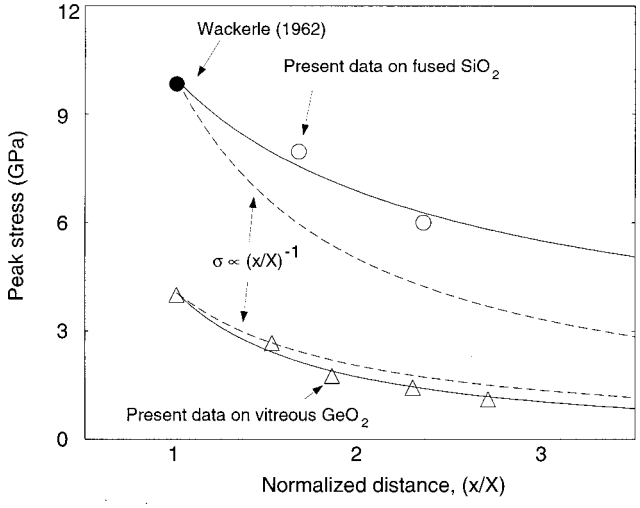

FIG. 10. Elastic shock wave amplitude vs propagation distance in fused SiO_2 and vitreous GeO_2 under spherical impact. The solid lines are best fit to the data [Eq. (3.5) for SiO_2 and Eq. (3.6) for GeO_2]. Dashed lines are for linear elastic wave decay.

IV. DISCUSSION OF DYNAMIC COMPRESSION DATA

A. Vitreous GeO_2 response to planar impact

Based on the present data (Fig. 7), the response of vitreous GeO_2 under planar shock loading is divided into three stress ranges: 0–4, 4–6, and 6 GPa and higher.

When the peak stress is below 4 GPa, the present data show that the compressibility of vitreous GeO_2 increases with increasing stress. Although compression measured by Smith *et al.*[24] is greater under hydrostatic loading (HL), the trend in the data is the same. The bulk and longitudinal wave velocities of vitreous GeO_2 under hydrostatic loading increase slowly with increasing pressure when the pressure is below 4 GPa (Fig. 12). However, the wave velocity under shock loading has a significant drop in this stress interval. When the shock stress is close to 4 GPa, the precursor wave

Downloaded 21 Dec 2005 to 131.215.225.171. Redistribution subject to AIP license or copyright, see http://jap.aip.org/jap/copyright.jsp

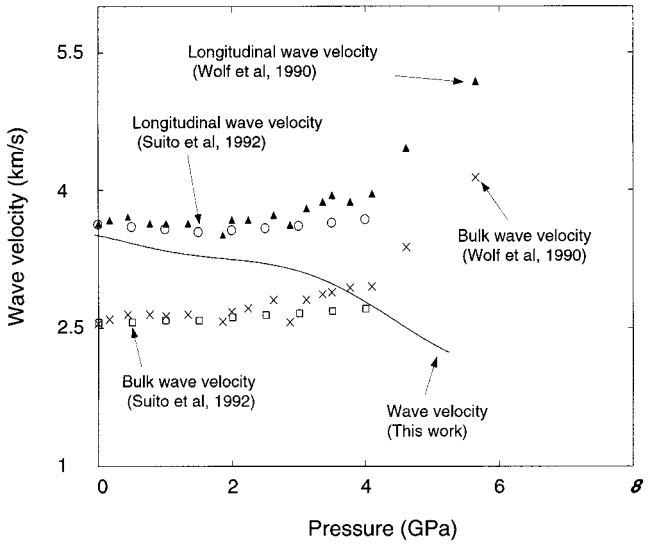

FIG. 12. Longitudinal and bulk wave velocities vs pressure. The data of Refs. 32 and 19 were obtained ultrasonically and via Brillouin scattering, respectively.

velocity approaches the bulk wave velocity under hydrostatic loading. In general, a ramp wave results from densification processes that may occur upon compression of long chain structures in glass.[25] Possibly the shear stresses which develop under shock loading may assist glass densification.[26]

When the peak stress is between 4 and 6 GPa, the compressibility increases dramatically under both planar impact and hydrostatic loading (Fig. 7). Smith *et al.*[24] found that the deformation is not reversible when pressure is higher than 4 GPa under hydrostatic loading. Wolf *et al.*[17] noted that heterogeneities with dimensions <0.5 μm appear in vitreous GeO_2 when hydrostatic pressure is >4 GPa. He suggested that a new (sixfold coordinated) phase starts to nucleate at 4 GPa. Shock recovery experiments conducted upon fused quartz yielded blocks of untransformed fused quartz surrounded by thin layers of remelted material when samples were exposed to shock pressures higher than the HEL of fused quartz.[27] Grady[28] suggested that the increase of compressibility under shock loading of fused quartz results from fracture nucleation, growth, followed by melting along microshear faults produced upon under shock loading.

When peak impact stress is >6 GPa, a steep fronted normal shock wave in GeO_2 forms. Shock wave formation implies that the compressibility of vitreous GeO_2 starts to decrease with increasing stress above 6 GPa. When shock stress is higher than $\sim$15 GPa, the vitreous GeO_2 compression data closely match that of rutile phase GeO_2 (Ref. 18) (Fig. 7). At this pressure it appears that the phase transition from fourfold to sixfold GeO_2 is completed. Therefore, we conclude that the phase transition to rutile phase in vitreous GeO_2 starts at $\sim$4 GPa and is completed in the pressure range of 14 to 16 GPa. Durben and Wolf[16] and Smith *et al.*[24] also inferred that the four-to sixfold GeO_2 transition also occurred between 5.6 and 13 GPa under quasistatic loading.

B. Similarities between GeO_2 and SiO_2 response under shock loading

Because the features of stress-wave profiles reveal changes of deformation processes during shock loading, it is possible that similarities in wave profile structure and pressure-volume relation (P-V relation) appear for materials with similar structure. Vitreous GeO_2 has a similar structure to fused SiO_2, and approximately also to soda-lime glasses.[25] Therefore, we examine the shock wave profiles and P-V relation similarities among these glasses.

1. Features of stress wave profiles

Bourne and Rosenberg[29] divided soda-lime glass response under planar impact into three stress regimes: 0–4, 4–6, and >6 GPa based on their experimental data. In addition, their results show that a ramp precursor appears with a maximum stress of 4 GPa and peak particle velocity of 320 m/s in soda-lime glass. Wackerle[3] and Barker and Hollenbach[30] found that shock wave profile in fused SiO_2 under shock loading is composed of a leading elastic shock precursor, and then a deformation shock wave. Sugiura *et al.*[31] further subdivided the stress-wave profile in fused SiO_2 into four waves, i.e., leading ramp precursor, elastic wave, ramp wave, and then shock wave. The leading ramp precursor in fused SiO_2 has an amplitude of 4 GPa (Refs. 3 and 30). The present results show that the leading ramp precursor in vitreous GeO_2 also has a amplitude of 4 GPa and particle velocity of 333 m/s. The above experimental data of fused SiO_2, vitreous GeO_2, and soda-lime glass show that a similarity appears on both stress-wave profiles (ramp precursor, ramp wave, and shock wave) and on the amplitude and particle velocity of leading precursor ($\sim$4 GPa and $\sim$320 m/s in all three glasses). These similarities probably result from very similar deformation processes in the materials. The experimental data indicate that the only difference on stress-wave profiles is that an elastic wave follows the leading precursor in SiO_2 but not in GeO_2. This may reflect the effects of the stronger bond in SiO_2.[15]

2. Equations of state of GeO_2 and SiO_2

Since vitreous GeO_2 has the same structure as fused SiO_2,[25] and Ge and Si ions demonstrate the same valence ($+4$) it is expected that on a per atom basis, the energy needed to induce phase change in the two materials should be similar. If we simply use the density ratio to scale the pressures in GeO_2 and SiO_2, P_G and P_S,

$$P_G = \frac{P_S \rho_S}{\rho_G}, \tag{4.1}$$

where ρ_G and ρ_S are vitreous GeO_2 and fused SiO_2 density, respectively. Figure 13 shows the comparison between fused SiO_2 and vitreous GeO_2 P-V relations under shock compression. Both of the P-V relations are aligned so that the densities of rutile and vitreous phase coincide. The pressure axis for SiO_2 is scaled down using Eq. (4.1). When the shock pressure is between 10 to 30 GPa, the pressure in fused SiO_2 (Refs. 23 and 19) appears slightly higher than suggested by Eq. (4.1). Both Refs. 28 and 13 indicated that the possible misinterpretation of the SiO_2 data exists. The shock wave

Downloaded 21 Dec 2005 to 131.215.225.171. Redistribution subject to AIP license or copyright, see http://jap.aip.org/jap/copyright.jsp

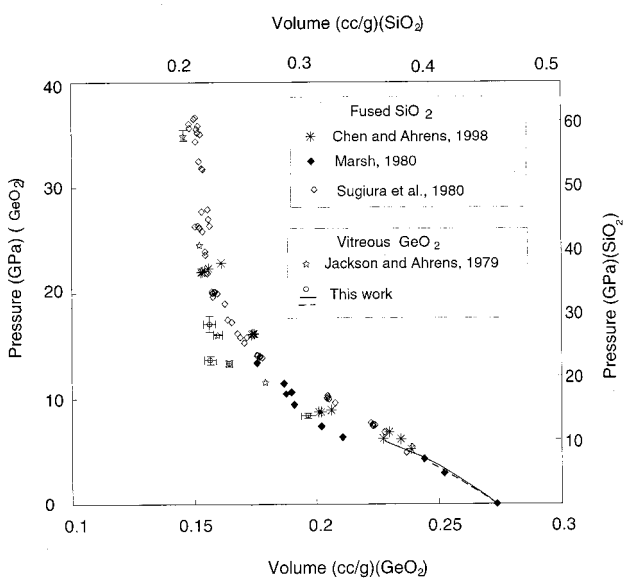

FIG. 13. Pressure vs volume for vitreous GeO_2 and SiO_2. Plots for SiO_2 and GeO_2 are aligned so that initial volume and the volume for rutile phase are coincident. The pressure axis for SiO_2 is scaled down by the ratio of initial densities of SiO_2 to GeO_2.

velocity in the 10–30 GPa pressure range was measured and reported as nearly a constant.[23] However, the stress-wave profile measurements[28,31] suggest that a single wave is not stable in this pressure range. The shock wave velocity appears to be slightly lower than that listed by Marsh.[23] In spite of this problem, Fig. 13 demonstrates a similarity of P-V relations of fused SiO_2 and vitreous GeO_2. This similarity demonstrates that the response of vitreous GeO_2 under relative low shock pressure appears to be similar to the response of fused SiO_2 at higher pressures. It has been long recognized that crystal chemically similar oxides such as GeO_2 and SiO_2 share many system properties.

V. DISCUSSION OF SHOCK WAVE ATTENUATION

A. Elastic wave decay

Two different elastic waves, linear and nonlinear, are defined generally as $\partial C/\partial\sigma=0$, and $\partial C/\partial\sigma\neq 0$, respectively ($C$ is the longitudinal elastic wave velocity and σ is stress). Elastic wave decay rate depends on both $\partial C/\partial\sigma$ and initial conditions (supported and nonsupported). In order to discuss this in detail, we first derive an approximate expression for spherical elastic wave propagation. Assuming that the center of a thin layer spherical wave is at x with stress σ, the leading and tailing edges of the layer are at $x+\Delta x/2$ and $x-\Delta x/2$ with stress $\sigma+\Delta\sigma/2$ and $\sigma-\Delta\sigma/2$ in which $\Delta\sigma=\sigma(x+\Delta x/2)-\sigma(x-\Delta x/2)$, respectively. When the layer center moves to $x+dx$, the locations of the leading and tailing edges of the layer are at x_l and x_t, respectively. Here

$$x_l=x+\Delta x/2+\left[C(\sigma)+\left(\frac{\partial C}{\partial\sigma}\right)\frac{\Delta\sigma}{2}\right]\frac{dx}{C}, \tag{5.1}$$

$$x_t=x-\Delta x/2+\left[C(\sigma)-\left(\frac{\partial C}{\partial\sigma}\right)\frac{\Delta\sigma}{2}\right]\frac{dx}{C}. \tag{5.2}$$

When the wave is centered at $x+dx$, the thickness of the layer is

$$\Delta x(x+dx)=x_l-x_t=\Delta x(x)+\left(\frac{\partial C}{\partial\sigma}\right)\Delta\sigma\frac{dx}{C}. \tag{5.3}$$

Then,

$$\frac{d\Delta x}{dx}\approx\frac{\Delta x(x+dx)-\Delta x(x)}{dx}=\left(\frac{\partial C}{\partial\sigma}\right)\frac{\Delta\sigma}{C}. \tag{5.4}$$

For a spherical shock wave, energy conservation requires

$$x^2\Delta x u^2=\text{const}, \tag{5.5}$$

where u is particle velocity at the center of the layer. After differentiating Eq. (5.5) with respect to x, we have

$$\frac{du}{dx}=-\frac{u}{x}\left(1+\frac{x}{2\Delta x}\frac{d\Delta x}{dx}\right). \tag{5.6}$$

Substituting Eq. (5.4) into Eq. (5.6) yields the particle velocity decay rate as

$$\frac{du}{dx}=-\frac{u}{x}(1+K_d x), \tag{5.7}$$

where $K_d=1/2\Delta x(\partial C/\partial\sigma)\Delta\sigma/C$. In general, K_d is a function of C, x, and u. Therefore, the particle velocity decay rate depends on wave propagation history.

For a very short propagation distance from x to x_1, K_d can be approximated to be a constant. Then, integration of Eq. (5.7) gives

$$\frac{u(x_1)}{u(x)}=\frac{x}{x_1}d_r, \tag{5.8}$$

where $d_r=\exp[-K_d(x_1-x)]$.

For a supported nonlinear elastic wave, $\Delta\sigma<0$. When $\partial C/\partial\sigma>0$,

$$K_d<0 \quad\text{and}\quad \frac{d\Delta x}{dx}<0. \tag{5.9}$$

When $\partial C/\partial\sigma<0$,

$$K_d>0 \quad\text{and}\quad \frac{d\Delta x}{dx}>0. \tag{5.10}$$

Equations (5.9) and (5.10) indicate that (1) for a material with $\partial C/\partial\sigma>0$, a nonlinear elastic wave decays less rapidly than that of a linear elastic wave by a ratio of d_r and the wave width decreases with propagation distance, and (2) for a material with $\partial C/\partial\sigma<0$, elastic wave decays more rapidly than that of a linear elastic wave by a ratio of d_r and the width increases with propagation distance.

For a nonsupported nonlinear elastic wave, $\Delta\sigma>0$ when $\partial C/\partial\sigma>0$, and $\Delta\sigma<0$ when $\partial C/\partial\sigma<0$. When $\partial C/\partial\sigma>0$,

$$K_d>0 \quad\text{and}\quad \frac{d\Delta x}{dx}>0. \tag{5.11}$$

When $\partial C/\partial\sigma<0$,

$$K_d>0 \quad\text{and}\quad \frac{d\Delta x}{dx}>0. \tag{5.12}$$

Downloaded 21 Dec 2005 to 131.215.225.171. Redistribution subject to AIP license or copyright, see http://jap.aip.org/jap/copyright.jsp

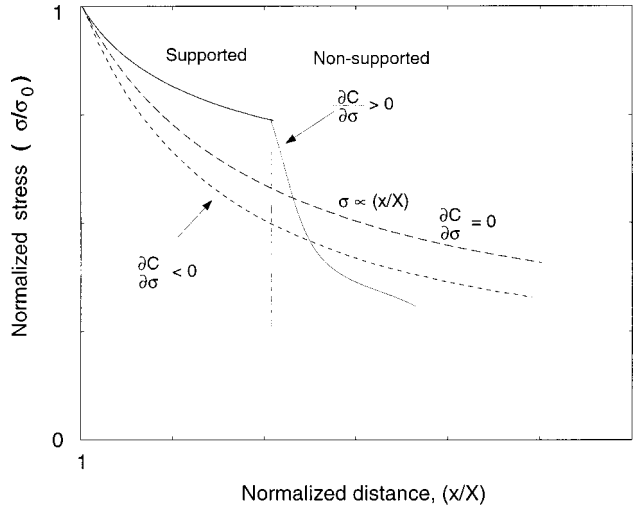

FIG. 14. Spherical elastic shock amplitude normalized by impact pressure at impact surface vs propagation distance normalized by spherical impactor radius.

Equations (5.11) and (5.12) show that for a material with $\partial C/\partial\sigma>0$ or $\partial C/\partial\sigma<0$, elastic wave decay is more rapid than that of a linear elastic wave by a ratio of d_r and the wave width increases with propagation distance. Figure 14 shows the relative decay rate of elastic waves of varying stress amplitude under three different conditions.

When peak stress is below elastic limit, the relation between stress and specific volume under impact and hydrostatic loading conditions is shown in Fig. 7 for vitreous GeO_2 (this work and Ref. 24) and Fig. 15 for fused SiO_2.[1] Figure 15 indicates that the compressibility of fused SiO_2 in the elastic deformation regime decreases with increasing stress under both uniaxial strain shock loading and hydrostatic loading, i.e., $\partial C/\partial\sigma>0$ when stress is higher than 4 GPa. Therefore, on the basis of Eq. (5.8), the decay of a supported elastic wave is expected to occur less rapidly than that of a linear elastic wave. The present experimental data [Eq. (3.5)] support this conclusion. For vitreous GeO_2, Fig. 7 indicates that the compressibility increases in elastic regime under both shock and hydrostatic loading, i.e., $\partial C/\partial\sigma<0$. Therefore, the supported elastic wave must decay faster than a linear elastic wave based on Eq. (5.8). The present data [Eq. (3.6)] agree with this prediction.

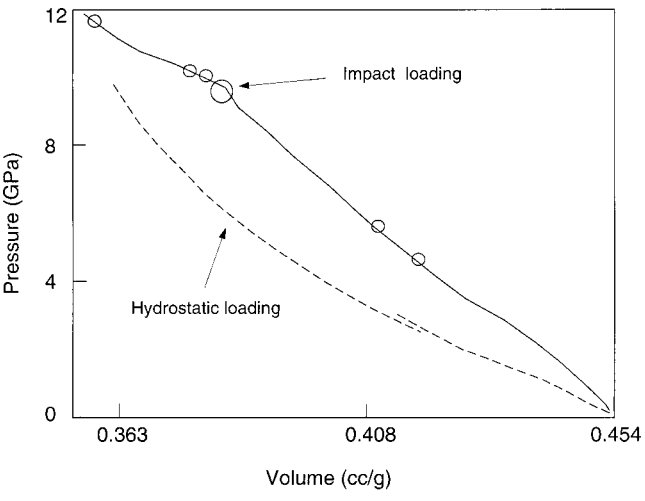

FIG. 15. Shock pressure vs volume of fused SiO_2 from Ref. 1.

B. Spherical shock wave decay

For a spherical shock wave, the same derivation in the above section can be followed. The particle velocity of a spherical shock wave decays according to

$$\frac{u(x_1)}{u(x)}=\frac{x}{x_1}\exp[-K_p(x_1-x)], \tag{5.13}$$

where

$$K_p=\frac{1}{2\Delta x}\left(\frac{\partial D}{\partial p}\right)_p\frac{\Delta p}{D}, \tag{5.14}$$

where Δp is the pressure difference at the leading and tailing edges of a shock wave layer. Because $\partial D/\partial p>0$ is the necessary condition for forming shock waves, $K_d<0$ for supported shock waves ($\Delta p<0$) and $K_d>0$ for nonsupported shock waves ($\Delta p>0$). Therefore, a supported shock wave decays less rapidly than a linear elastic wave, and a nonsupported shock wave decays more rapidly than a linear elastic wave. The slow decay rate of the supported shock wave results from the energy transfer between the tailing and leading edges. From both experimental and numerical calculations, it was found that the spherical shock wave decays very slowly near the impact site.[20] The slow decay is expected to be largely the result of the slow geometric spreading.[20] However, the above discussion suggests that a contribution to the slow decay results from energy exchange between the wave front and wave tail.

The above discussion only considers the decay due to geometry and supported conditions. In general, shock wave decay is controlled by several processes, such as, geometric effect, release wave, and velocities (which in turn are controlled by phase transformation, plastic deformation, and interaction between shock and elastic waves). In vitreous GeO_2, Chen *et al.*[19] found using numerical simulations that spherical wave decay follows a law such that $P\sim x^{\alpha}$ where α is -1.15 when pressure is below 8 GPa and -2.72 when pressure is higher than 8 GPa. The -2.72 value of α is believed to be due to irreversible phase transitions in GeO_2 when the pressure is over 8 GPa. The shock wave decay shown in Fig. 11 results from four major processes that are (1) geometrical spreading, (2) release wave overtaking, (3) phase transition, and (4) the transformation of shock wave energy to precursor energy. Therefore, the decay rate of a spherical shock wave in vitreous GeO_2 under present experimental conditions should change dramatically with peak pressure or propagation distance as labeled by stages A, B, C, and D in Fig. 11. During stage A, because the shock wave is supported, the shock wave decays slowly. During stage B, the release wave starts to overtake the shock wave. Because of the phase transition, the release wave velocity depends on both the percentage of the high density phase and the reversibility of the phase transition under release,[19] the shock wave decay rate changes dramatically in the pressure range of 6 to 14 GPa. During stage C, the shock wave decay rate changes

Downloaded 21 Dec 2005 to 131.215.225.171. Redistribution subject to AIP license or copyright, see http://jap.aip.org/jap/copyright.jsp

again due to the ramp-wave structure in this pressure range of 4 to 6 GPa. During stage D, the shock wave disappears.

Based on the above discussion, the shock wave decay rate cannot be explained simply using $P \sim x^{-\alpha}$ in the pressure range where a material is undergoing a phase transition. The details of shock wave decay should be based on phase transition dynamics under loading and unloading.

VI. CONCLUSIONS

(1) Vitreous GeO_2 demonstrates an elastic precursor with an amplitude of 4 GPa and a particle velocity of 333 m/s. The wave velocity decreases from the initial longitudinal velocity of 3.5 km/s at ambient pressure to the bulk wave velocity of ~2.9 km at ~4 GPa. A ramp wave follows the elastic precursor with an amplitude ~2 GPa. Within this pressure interval, compressibility increases significantly. The wave velocity drops to ~2.3 km/s at ~6 GPa. It is possible that partial melting and/or fracture and/or new phase formation may be occurring in this shock pressure range. A normal shock wave forms when the peak shock stress is higher than 6 GPa. Based on present data and Jackson and Ahrens' data,[18] the shock velocity-particle-velocity Hugoniot relation for vitreous GeO_2 is $D(\text{km/s}) = 0.917 + 1.711u$ for $u > 0.6$ km/s.

(2) When the shock stress is higher than ~15 GPa, vitreous GeO_2 compression data closely match the specific volume of rutile-structured GeO_2.[18] Therefore, the phase change from four to sixfold GeO_2 begins at ~4 GPa and is completed at ~15 GPa.

(3) A similarity between the pressure-volume relations for fused SiO_2 and GeO_2 can be demonstrated by multiplying the shock stress in SiO_2 by the ratios of the densities of SiO_2 (glass) to GeO_2 (vitreous) when the specific volumes at the onset and completion of the four to sixfold coordination phase change are made to coincide. Comparison of wave profiles of fused SiO_2, vitreous GeO_2, and soda-lime glass demonstrate that the ramp elastic precursor in the three materials has approximately the same amplitude (~4 GPa) and particle velocity (~330 m/s).

(4) Spherical impact experiments demonstrate that a supported spherical elastic wave in fused SiO_2 decays less rapidly than that of a linear elastic wave when the elastic wave amplitude is higher than 4 GPa, and a supported spherical elastic wave in vitreous GeO_2 decays more rapidly than that of a linear elastic wave. Based on a simple analysis of elastic wave propagation, it was found that the different decay rate of a spherical elastic wave in fused SiO_2 and vitreous GeO_2 results from the compressibility variation with stress in these materials. The energy exchange among supported shock waves may contribute to the very slow decay near the impact site as observed and calculated.[20] The experimental data indicate that the phase transition in GeO_2 has a major effect on spherical shock wave decays as predicted previously.[19]

ACKNOWLEDGMENTS

Research was supported by NSF, NASA, and ARO. We appreciate the experimental support for E. Gelle and M. Long. Contribution No. 8843, Division of Geological and Planetary Science, California Institute of Technology, Pasadena, California.

[1] J. Wackerle, J. Appl. Phys. **33**, 922 (1962).
[2] R. Fowles and R. F. Williams, J. Appl. Phys. **37**, 360 (1970).
[3] T. J. Ahrens and V. G. Gregson, Jr., J. Geophys. Res. **69**, 4839 (1964).
[4] R. G. McQueen, S. P. Marsh, and J. N. Fritz, J. Geophys. Res. **72**, 4999 (1967).
[5] T. J. Ahrens, C. F. Peterson, and J. T. Rosenberg, J. Geophys. Res. **74**, 2727 (1969).
[6] E. C. T. Chao, J. J. Fahey, J. Littler, and D. J. Milton, J. Geophys. Res. **67**, 419 (1962).
[7] D. E. Grady, W. J. Murri, and G. R. Fowles, J. Geophys. Res. **79**, 332 (1974).
[8] M. A. Podurets, G. V. Simakov, and R. F. Trunin, Izvestiya, Earth Phys. **24**, 267 (1988).
[9] L. C. Chhabildas and J. M. Miller, SAND 85-1092, Sandia National Laboratory, Albuquerque, NM, 1985.
[10] Y. N. Zugin, in *Shock Compression of Condensed Matter—1995*, edited by S. C. Schmidt and W. C. Tao, AIP Conf. Proc. No. **370** (AIP, Woodbury, NY, 1996), pp. 97–100.
[11] J. W. Swegle, J. Appl. Phys. **68**, 1563 (1990).
[12] L. M. Truskinovskiy, Geokhimiya (Engl. trans.) **3**, 443 (1984).
[13] D. Turnbull, Solid State Phys. **3**, 225 (1956).
[14] E. M. Stolper and T. J. Ahrens, Geophys. Res. Lett. **14**, 1231 (1987).
[15] J. P. Itie, A. Polian, G. Calas, J. Petiau, A. Fontaine, and H. Tolentino, Phys. Rev. Lett. **63**, 398 (1989).
[16] D. J. Durben and G. H. Wolf, Phys. Rev. B **43**, 2355 (1991).
[17] G. H. Wolf, S. Wang, C. Herbest, D. Durben, W. Oliver, Z. Kang, and K. Halvorson, in *High-Pressure Research: Application to Earth and Planetary Science*, edited by Y. Syono and M. H. Manghnani (Terra Scientific, Tokyo, 1992), pp. 503–517.
[18] I. Jackson and T. J. Ahrens, Phys. Earth Planet. Inter. **20**, 60 (1979).
[19] G. Q. Chen, T. J. Ahrens, Wenbo Yang, and J. K. Knowles, J. Mech. Phys. Solids **47**, 763 (1999).
[20] T. J. Ahrens and J. D. O'Keefe, in *Impact and Explosion Cratering*, edited by D. J. Roddy, R. O. Pepin, and R. B. Merrill (Pergamon, New York, 1977), pp. 639–656.
[21] Z. Rosenberg, D. Yaziv, and Y. Partom, J. Appl. Phys. **51**, 3702 (1980).
[22] C. Liu, Ph.D. thesis, Caltech, 1999.
[23] *LASL Shock Hugoniot Data*, edited by S. P. Marsh (University of California Press, Berkeley, CA, 1980), pp. 321–324.
[24] K. Smith, E. Shero, A. Chizmeshya, and G. Wolf, J. Chem. Phys. **102**, 6851 (1995).
[25] H. Scholze, *Glass* (Springer, New York, 1991).
[26] S. Sundaram Ph.D. thesis, Brown University, 1998.
[27] A. V. Anan'in, O. N. Breusov, A. N. Dremin, S. V. Pershin, and V. F. Tatsii, Combust., Explos. Shock Waves **10**, 372 (1974).
[28] D. E. Grady, Mech. Mater. **29**, 181 (1998).
[29] N. K. Bourne and Z. Rosenberg, in *Shock Compression of Condensed Matter–1995*, edited by S. C. Schmidt and D. Tao, AIP Conf. Proc. No. **370** (AIP, New York, 1996), pp. 567–573.
[30] L. M. Barker and R. E. Hollenbach, J. Appl. Phys. **41**, 4208 (1970).
[31] H. Sugiura, K. Kondo, and A. Sawaoka, J. Appl. Phys. **52**, 3375 (1980).
[32] K. Suito, M. Miyoshi, T. Sasakura, and H. Fujisawa, in *High-Pressure Research: Application to Earth and Planetary Sciences*, edited by Y. Syono and M. Manghnani (Terra Scientific, Tokyo, 1992), pp. 219–225.

Downloaded 21 Dec 2005 to 131.215.225.171. Redistribution subject to AIP license or copyright, see http://jap.aip.org/jap/copyright.jsp